Alternating anion-cation bond strengths in $CdGeAs_2$: Application to the family of ternary pnictides

J. Pascual
Departament Física, Universitat Autònoma de Barcelona, and Institut de Ciència de Materials de Barcelona, 08193 Bellaterra, Spain

J. Pujol
Departament d'Enginyeria Mecànica, Escola Tecnica Superior d'Enginyers Industrials de Terrassa, Universitat Politècnica de Catalunya, 08222 Terrassa, Spain

L. Artus
Institut de Ciència de Materials de Barcelona, Consell Superior d'Investigacions Científiques, calle Martí i Franquès s/n, 08028 Barcelona, Spain

J. Camassel
Groupe d'Etudes des Semiconducteurs, Case Postale 74, Université des Sciences et Techniques du Languedoc, 34095 Montpellier CEDEX 5, France
(Received 20 November 1990)

We have investigated in great detail the low-temperature infrared (ir) transmission and polarized-Raman-scattering spectra of $CdGeAs_2$. We identified all vibrational modes predicted from group-theory arguments and compared them with predictions of three- and four-parameter valence-force-field models. Assuming only nearest-neighbor interactions for the two different series of anion-cation bonds that define the ternary pnictide structure, we have found the resulting series of force constants to be in very good agreement with predictions of the semiempirical tight-binding method. This results in an inverse scaling of the force constants versus the fourth power of the bond length which, together with the use of a simple molecular model, has provided enough physical insight to allow simple but accurate predictions to be made. This shows that there is a one-to-one correspondence between the identity of chemical species that enter a given compound and the experimental phonon frequencies that dominate the ir and Raman spectra. This correspondence is found to hold true for the whole family of ternary pnictides.

I. INTRODUCTION

The ternary analogs of ZnS-type (zinc-blende-structure) semiconductors, with the general formula ABC_2, form a large family of compounds. They crystallize in the so-called chalcopyrite structure (space group D_{2d}^{12}, or $I\bar{4}2d$) and have long been studied for their nonlinear optical properties.[1] More recently, they have also emerged as the prototypes of a class of intermediate materials between the pure binary compounds, such as GaAs and InAs, for which one single series of A—B tetrahedral bonds defines a perfect regular arrangement and the family of *ordered* ternary and quaternary alloys,[2] for which different series of tetrahedral bonds have to match with one another. This includes the synthetic $(AC)_1/(BC)_1$ strained superlattices[3] and, because such systems are increasingly being considered for device applications,[4] a detailed understanding of the tetrahedral bonding has become a matter of considerable technological interest.

Similar to the superlattice materials, in the ternary chalcopyrite semiconductors, also, *naturally ordered* series of alternating A—C and B—C bonds do simultaneously exist. Moreover, in both cases, all specific effects must correlate with the standard chemistry of the constituent atoms. Since there are 58 predicted ternary analogs of the ZnS-type semiconductors (of which 36 have been synthesized and 22 more are, up to now, only supported by theoretical predictions[5]), they constitute a very broad field for investigation (both theoretically and experimentally) as was first recognized by Jaffe and Zunger.[5–8] Emphasizing the peculiarities of the alternating-bond scheme, they discussed in detail the structural parameters, the chemical trends, and the band-gap anomalies for (i) the ternary analogs $A^{\mathrm{I}}B^{\mathrm{III}}C_2^{\mathrm{VI}}$ of the II-VI binary compounds $A^{\mathrm{II}}B^{\mathrm{VI}}$ (the so-called "group-I" chalcopyrites[6]) and (ii) the ternary analogs $A^{\mathrm{II}}B^{\mathrm{IV}}C_2^{\mathrm{V}}$ of the III-V binary semiconductors $A^{\mathrm{III}}B^{\mathrm{V}}$ (the so-called "group-II" chalcopyrites, or ternary pnictides[7]). They showed that the conservation of tetrahedral bonds (CTB), admixed by p-d hybridization effects for the noble-metal compounds, played a key role in the geometry of the material and was the main source of lattice distortions.[5,8]

How much of this simple viewpoint was reflected in considering the lattice dynamics was not clearly established. On the contrary, there exist reports supporting a folded-zone scheme[1] in which the specific effects associat-

ed with the two different cation species are not taken into account. To clear up this point, we have attempted a recent systematic study of the lattice dynamics of group-I $A^{I}B^{III}C_2^{VI}$ and group-II $A^{II}B^{IV}C_2^{V}$ chalcopyrites.[9,10] We investigated $AgGaSe_2$ and $CdGeP_2$, among others, and, starting from the folded-zone scheme in which both A and B cations have been averaged to one single $(A+B)/2$ chemical species, we could weigh the different effects of mass differences, tetrahedral distortion, tetragonal compression and, finally, changes in force constants. By investigating in great detail the long-wavelength phonons in both compounds, and comparing systematically with the results of our theoretical predictions, we could show the following.

(i) For the cases of $AgGaSe_2$ and $CdGeP_2$, two different series of anion-cation bonds give two different series of well-identified ir and Raman-active frequencies in the high- to intermediate-frequency range.

(ii) With respect to the closest fictitious analogs ($CdZnSe_2$ and $InGaP_2$, respectively), the change in bond strength depends on whether we are considering the heavy or light cations. In the first case (heavy cations) we have found only smooth bonds, weakly sensitive to the chalcopyrite substitution. In units of 10^3 dyn/cm, the corresponding force constants were $\alpha=18.87$ and $\beta=0.80$ for Ag—Se bonds in $AgGaSe_2$ (to be compared with $\alpha=17.63$ and $\beta=0.82$ estimated for cubic CdSe) and $\alpha=32.9$ and $\beta=3.65$ for Cd—P bonds in $CdGeP_2$ (to be compared with $\alpha=34.8$ and $\beta=2.5$ for cubic InP). Those relative changes were typically 6%. In the second case (light cations) where all bonds are shorter, they appeared more sensitive [and even more so for the (group-I) ternary chalcopyrites than for the (group-II) ternary pnictides]. We have found the following values: $\alpha=36.93$ and $\beta=0.80$ for Ga—Se bonds (to be compared with $\alpha=24.53$ and $\beta=3.88$ for ZnSe) and $\alpha=44.9$ and $\beta=3.65$ for Ge—P bonds (to be compared with $\alpha=39.2$ and $\beta=4.7$ for GaP). This constituted renormalizations of 50% and 15%, respectively. This marked asymmetry of bond strengths, noticed in both compounds, explains the appearance of well distinct optical bands and the so-called[9,10] "hard-bond–smooth-bond" features.

In this work, we focused on the parent compound $CdGeAs_2$ to see how much of the preceding results can be used to perform systematic predictions. We first note that, from previous infrared (ir) studies performed at room temperature in the experimental range 50–500 cm^{-1}, only $2\Gamma_4$ and $5\Gamma_5$ modes were known.[11,12] Moreover, no Raman experiments were reported and $1\Gamma_1$, $3\Gamma_3$, $1\Gamma_4$, and $1\Gamma_5$ frequencies predicted by group theory were missing. Accordingly, since no significant comparison with theoretical predictions could be done, we first complement the existing experimental data. Performing, at low temperature, infrared transmission and Raman spectroscopy, we resolved all Raman- and ir-active frequencies. Then we will discuss the results in light of the valence-force-field (VFF) model[9,10,13] and show the close analogy which ties together $CdGeAs_2$ and $AgGaSe_2$ with respect to $CdGeP_2$. This is nothing but an effect due to the relative values of atomic masses. Finally, we will discuss the change in force constants through the isoelectronic series: $InGaAs_2$ to $CdGeAs_2$ and $InGaP_2$ to $CdGeP_2$ and show that all agree satisfactorily with the predictions of a simple scaling law which assumes an inverse proportionality of the bond strength to the bond length. Because no free parameter is introduced, and only the standard prescriptions of the semiempirical tight-binding method (TBM) have been taken into account,[14] we obtain enough physical insight to allow simple, but accurate, molecular predictions to be made for phonons identified with a chemical bond. This is true for the whole family of ternary pnictides.

II. EXPERIMENTAL RESULTS

The ternary chalcopyrite semiconductors crystallize in the D_{2d}^{12} space group and contain two formula units per primitive unit cell. At the center of the Brillouin zone, the symmetry of the crystal decouples the 24 vibrational modes into 15 nonzero (optical) frequencies and 2 acoustic components:

$$\Gamma=\Gamma_1+2\Gamma_2+3\Gamma_3+3\Gamma_4+6\Gamma_5+(\Gamma_4+\Gamma_5)_{ac} .$$

Among them $3\Gamma_4(z)$ and $6\Gamma_5(x,y)$ are polar modes, both ir and Raman active; $1\Gamma_1$ and $3\Gamma_3$ are nonpolar Raman-active modes and $2\Gamma_2$ are optically inactive.

As already mentioned, from infrared experiments reported at 300 K in the experimental range 50–500 cm^{-1}, only $2\Gamma_4$ and $5\Gamma_5$ modes could be resolved. This was true both in our work[12] and in the work of Ref. 11. Since the missing components should fall in the low-energy range and have small oscillator strengths, we have performed infrared transmission measurements at low temperature.

We have also checked the low-temperature reflectivity signal but no finite advantage could be gained over the room-temperature data. This was because of a reduced signal-to-noise ratio coming from both the presence of additional windows and the smaller optical aperture. As a consequence, we have systematically used in this work our room-temperature reflectivity spectra[12] to compare the series of Γ_4 and Γ_5 modes deduced from the ir spectra with the results of the Raman investigation.

A. Infrared transmission

Our experimental setup has been already described[9,15] and no additional detail will be given here. Collected through a 1-mm-thick sample with unpolarized light, a low-temperature transmission spectrum gives the typical absorbance intensity shown in Fig. 1(a). Clearly three modes are found at 42, 73, and 97 cm^{-1}, of which only one (97 cm^{-1}) appears also (at 93 cm^{-1}) in the room-temperature reflectivity spectrum. This is shown on Fig. 1(b). The theoretical predictions[13] indicate that the lower- and higher-energy components have Γ_5 symmetry and that the intermediate-energy one has Γ_4 symmetry. This is the standard ordering already reported[9,10] for $AgGaSe_2$ and $CdGeP_2$ and will be confirmed by further examination of the Raman data.

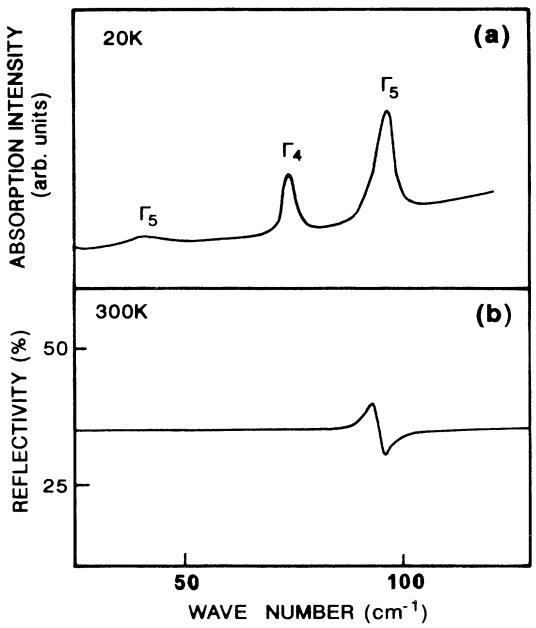

FIG. 1. (a) Unpolarized low-temperature absorption intensity collected through a 1-mm-thick sample; (b) room-temperature reflectivity spectrum, also collected with unpolarized light, on the same sample. In the first case, three modes resolve at 42, 73, and 97 cm^{-1}. They have been assigned to Γ_5, Γ_4, and Γ_5 symmetry, respectively. In the second case, only one mode resolves at 93 cm^{-1} and corresponds to the upper Γ_5 mode in the lowest band (see Fig. 3 and Table I).

B. Raman experiments

Concerning the Raman experiments, most experimental details have already been given[9,10] and only a few specific features relative to $CdGeAs_2$ need further discussions. First, because $CdGeAs_2$ is a small-band-gap semiconductor (0.57 eV at room temperature[16]), we could not work in the transparency region and only a backscattering configuration was used. Second, because the 5682-Å wavelength of the krypton-ion laser is close to the N_{1v}-N_{1c} transition (E_1-like transition in ZnS-type compounds[17]), we expected some resonant behavior. Since we knew, from the work of Ref. 18, that the E_1-like transitions give strong reflectivity structures centered at 2.20 and 2.05 eV at 8 and 300 K, respectively, a simple extrapolation indicates 2.17 eV at 77 K. Indeed, checking for different wavelengths, we could find a better signal-to-noise ratio when using the 5682-Å line (2.18 eV) of the Kr^+-ion laser. As a consequence, this line was used for the remaining part of this work, with an incident power kept below 300 mW in order to avoid damaging the samples.

1. Γ_4 modes

According to the selection rules discussed in Ref. 9, we have used a $\langle z|xy|\bar{z}\rangle$ configuration for the Γ_{4L} frequencies and, next, a $\langle x'|y'y'|\bar{x}'\rangle$ configuration (in which Γ_1

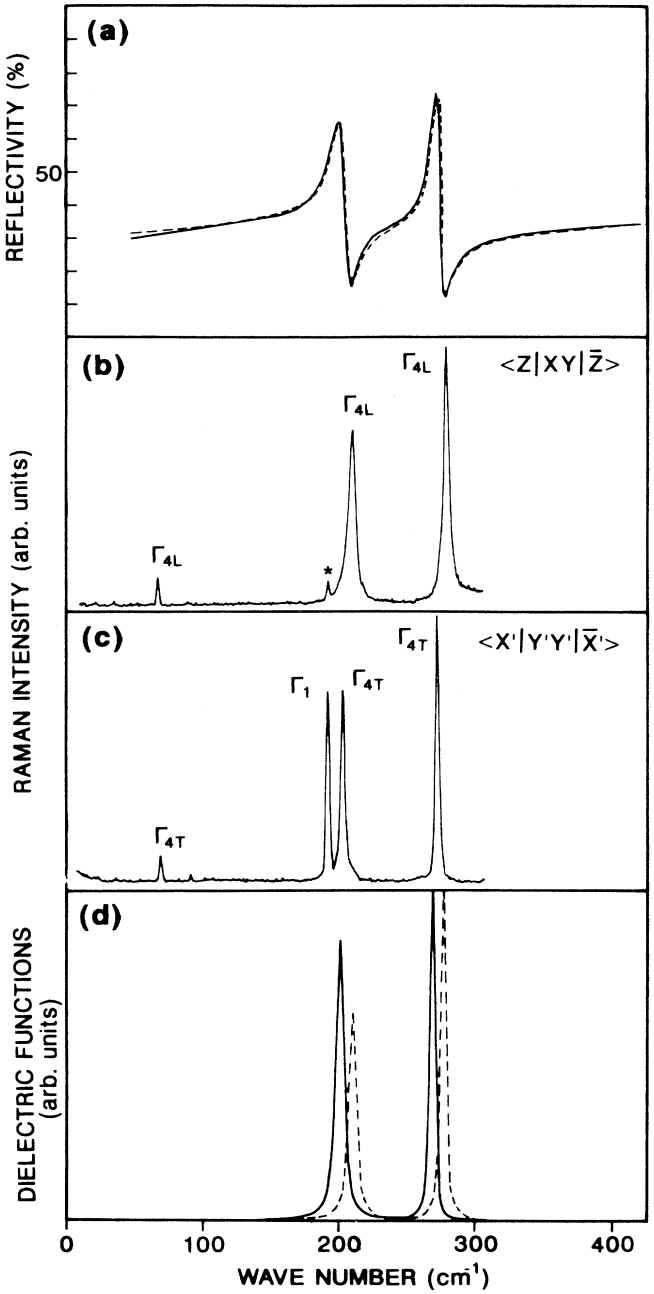

FIG. 2. Comparison of Γ_4 frequencies resolved in this work. (a) is a room-temperature reflectivity spectrum collected with light polarized in the configuration $E\|c$. The dashed line is a theoretical oscillator fit (least-mean-squares fit) using the series of parameters listed in Ref. 12; (b) is a Raman spectrum, collected at liquid-nitrogen temperature, in the backscattering $\langle z|xy|\bar{z}\rangle$ configuration. In this case, three longitudinal Γ_{4L} frequencies manifest at 73, 216, and 284 cm^{-1} (see Table I). Indicated by an asterisk is the forbidden Γ_1 component. It comes from imperfect selection rules. (c) refers to the transverse frequencies, also at liquid-nitrogen temperature. In this case, both the Γ_1 and Γ_{4T} modes are theoretically allowed and appear at 196 and 73 and 205 and 273 cm^{-1}, respectively. (d) is a plot of the dispersion of the two dielectric functions $\mathrm{Im}(\epsilon)$, solid line, and $\mathrm{Im}(-1/\epsilon)$, dashed line, obtained from the oscillator-fit parameters of Ref. 12 and corresponds to the room-temperature data illustrated in (a).

is also allowed) for the Γ_{4T} modes. Typical spectra are shown in Fig. 2. Also shown for comparison purposes are, first in Fig. 2(a), a room-temperature reflectivity spectrum collected on the same sample (solid line) and, second in Fig. 2(d), two plots of the dielectric functions $\mathrm{Im}(\epsilon)$ and $\mathrm{Im}(-1/\epsilon)$ (solid and dashed lines, respectively). Both were obtained from the least-mean-squares fit (LMSF) parameters listed in Ref. 12 and, for completeness, the corresponding theoretical reflectivity spectrum is shown in Fig. 2(a) (dashed line).

Consider, first, Fig. 2(b). We resolve $3\Gamma_{4L}$ frequencies at 284, 216, and 73 cm^{-1} which agree satisfactorily with the ir data of Figs. 2(a) and 2(d) and the Γ_4 absorption line displayed in Fig. 1(a). The small component noted by an asterisk, around 200 cm^{-1}, is the forbidden Γ_1 mode. It resolves clearly in Fig. 2(c), together with the Γ_{4T} frequencies. From this series of data, we resolve the Γ_1 mode at 196 cm^{-1} and confirm the Γ_{4T} frequencies at 273, 205, and 73 cm^{-1}, respectively.

For comparison purposes, we list in Table I the Raman and ir frequencies obtained in this work, together with the ir results of Refs. 11 and 12. Concerning the higher-energy Γ_4 modes, we notice a typical energy difference of 5 cm^{-1} between the room-temperature reflectivity data and the Raman modes which comes from the temperature dependence of the phonon spectrum. In both cases, however, the LO-TO-splitting agreement is within 3 cm^{-1}.

2. Γ_5 modes

We have selectively excited the Γ_{5L} and Γ_{5T} frequencies using the $\langle x|zy|\bar{x}\rangle$ and $\langle x'|zy'|\bar{x}'\rangle$ configurations, respectively. Typical experimental spectra are shown in Fig. 3 and the resulting LO-TO frequencies are listed in Table I.

Comparing with the ir data [see Figs. 3(a) and 3(d)], we find, again, a good overall agreement (see Table I). We notice also that, with the exception of two cases, 275–290

TABLE I. Comparison of experimental results obtained in different works.

	Frequency (cm^{-1})			
	Raman	ir	ir	ir
	77 K[a]	20 K[a]	300 K[b]	300 K[c]
Mode	TO (LO)	TO	TO (LO)	TO (LO)
Γ_1	196			
Γ_3	260			
	165			
	75			
Γ_{4T} (Γ_{4L})	273 (284)		270 (278)	270 (278)
	205 (216)		202 (211)	203 (210)
	73 (73)	73		
Γ_{5T} (Γ_{5L})	275 (290)		272 (283)	272 (280)
	259 (264)		257 (258)	255 (258)
	203 (209)		199 (202)	200 (206)
	160 (165)		157 (160)	159 (161)
	96 (97)	97	93 (93)	95 (98)
	46 (48)	42		

[a]In this work.
[b]In the work of Ref. 12.
[c]In the work of Ref. 11.

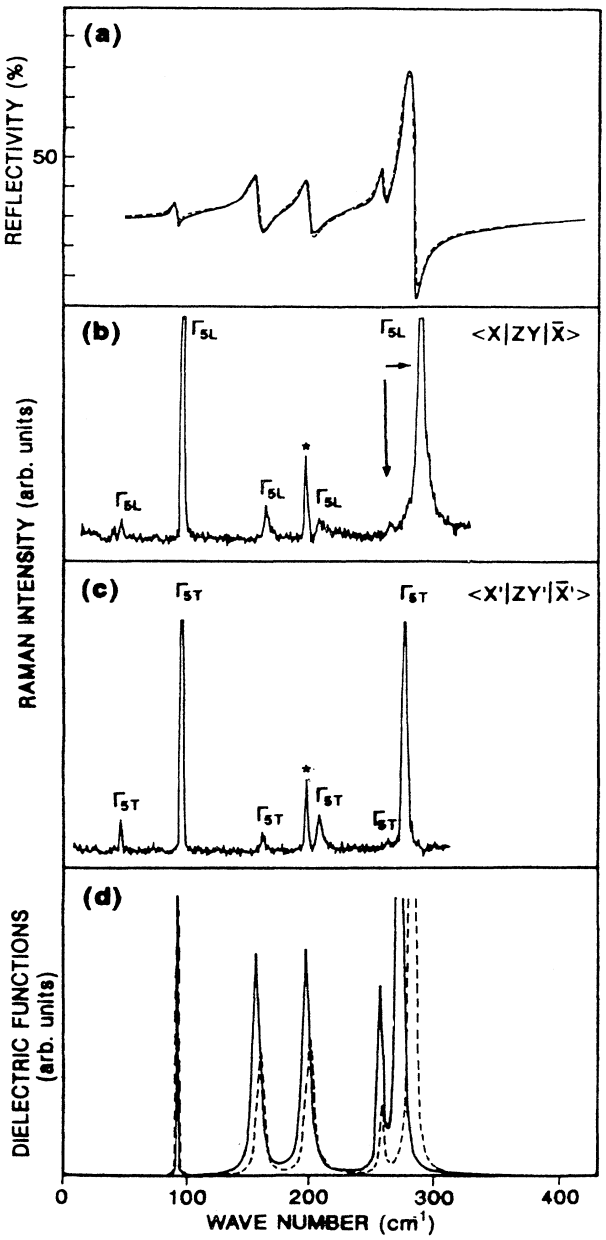

FIG. 3. Same as Fig. 2, but now for the Γ_5 modes. Again, (a) and (d) are room-temperature data and refer to the polarization E⊥c while (c) and (d) are Raman spectra collected at liquid-nitrogen temperature. In this case, only two modes have a strong Raman cross section; three are very weak and one, at about 260 cm^{-1}, is hardly resolved in both the Γ_{5L} (arrow) and Γ_{5T} configurations. Indicated by asterisks are Γ_1 components. For the sake of completeness, all experimental frequencies have been listed in Table I.

and 96–97 cm^{-1}, there are *no* very large experimental Raman cross sections. This causes the forbidden Γ_1 mode (indicated by asterisks) to appear on both experimental spectra. As already discussed (see Ref. 9), this comes from a partial breaking of the selection rules which is a constant feature when dealing with the ternary pnictide (group-II) and ternary chalcopyrite (group-I) semiconductors. Whether this comes more from the difficulty of growing large single crystals of very high quality or from intrinsic details of the resonance mechanism is not understood. In this respect, however, it seems that tuning the electronic excitation away from the fundamental edge results in somewhat better selection rules and less intensity of the Γ_1 mode with respect to the series of Γ_5 components (compare, for instance, with the corresponding spectra displayed in Refs. 9 and 10, respectively).

Concerning the small Raman cross section noted for the $4\Gamma_5$ modes at 259 (264), 203 (209), 160 (165), and 46 (48) cm^{-1}, we shall come back to this point later in Sec. III.

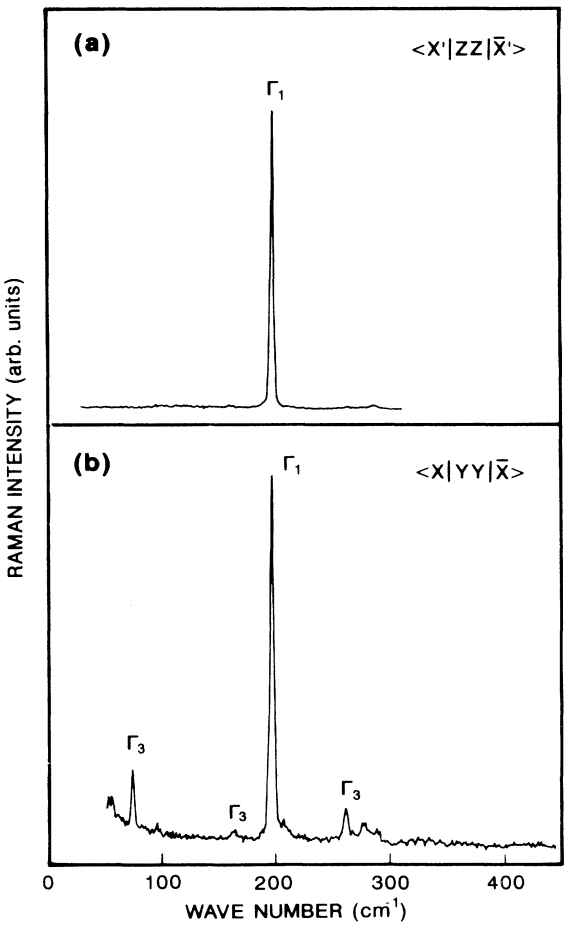

FIG. 4. Γ_1 and Γ_3 modes observed at liquid-nitrogen temperature, in the backscattering configuration. Notice the small Raman cross section associated with the weak Γ_3 mode at 165 cm^{-1} (see text).

3. *Nonpolar Γ_1 and Γ_3 modes*

Displayed in Fig. 4 are the Raman-scattering intensities observed for the nonpolar Γ_1 and Γ_3 modes, from the two different configurations $\langle x'|zz|\bar{x}'\rangle$ and $\langle x|yy|\bar{x}\rangle$, respectively. In both cases, the strong Γ_1 component dominates the spectra and the experimental value (196 cm^{-1}) confirms the data of Fig. 2(c). Two weaker Γ_3 modes appear, next, at 75 and 260 cm^{-1}, respectively. The third Γ_3 mode was very hard to resolve and assigned to the weak component observed at 165 cm^{-1}. This is, first, supported by theoretical predictions (see Sec. III) and, on the experimental side, seems reasonable because there is no artifact in this energy range [except a small Γ_{5L} mode which is already vanishingly small in the allowed configuration; cf. Table I and Fig. 3(b)].

The weak Raman intensity associated with the Γ_3 modes—especially the intermediate-energy one—is a common feature of the family of chalcopyrite compounds which again is not presently understood. It has been argued[19] that, similar to the more standard ZnS-type semiconductors, the Raman cross section is mainly determined by the band-gap modulation of the upper valence band and, since in a simple molecular model the topmost valence bands are made of p states of the anions (while the lowest conduction bands are made of empty states of the cations), one would expect weak (strong) Raman cross sections, provided that the phonon eigenstates are made of pure cationic (anionic) vibrations which hardly (strongly) modulate the upper states of the valence band. This should be true whatever the phonon symmetry is and we shall also come back to this point in Sec. III.

III. COMPARISON WITH THE THEORETICAL PREDICTIONS

Following our previous work,[9,10] we define two force constants per bond and, fitting the simple VFF model of Ref. 20 to the experimental data, we get the following.

(i) For Ge—As, $\alpha=40.26\times10^3$ dyn/cm and $\beta=7.90\times10^3$ dyn/cm.

(ii) For Cd—As, $\alpha=26.17\times10^3$ dyn/cm and $\beta=-1.61\times10^3$ dyn/cm.

The corresponding phonon frequencies have been listed in Table II. For the sake of simplicity, we have also studied a three-parameter model and, except for the lowest frequency range, we have found very similar results (see Table II again). Of course, because it is simpler, in the remaining part of this work we shall only focus on the three-parameter model.

Three points should be noted first.

(i) With respect to the phonon frequencies, most theoretical energy positions are within ±5% of the experimental values.

(ii) The larger discrepancies concern, first, a wrong phonon ordering for the two Γ_4-Γ_5 pairs around 205 and 275 cm^{-1} and, second, the theoretical position of the Γ_1 mode. While the calculation predicts 184 cm^{-1}, the Raman data give 196 cm^{-1}.

(iii) The overall grouping in three bands—already noted for $AgGaSe_2$ (Ref. 9) and $CdGeP_2$ (Ref. 10)—remains.

TABLE II. Comparison of experimental phonon frequencies (cm^{-1}) obtained in this work for $CdGeAs_2$ with different theoretical estimates. We have used four- and three-parameter valence-force-field (VFF) models and find a satisfactory agreement in both cases. The corresponding force constants are listed in units of 10^3 dyn/cm. Also listed for comparison purposes are simple molecular values (see Sec. IV).

Mode	Raman frequency	VFF four parameters	VFF three parameters	Molecular frequency
Γ_4	273	284	282	281
Γ_5	275	279	280	281
Γ_5	259	253	254	
Γ_3	260	250	249	
Γ_2		214	204	
Γ_5	203	209	208	207
Γ_4	205	208	206	207
Γ_1	196	183	184	197
Γ_5	160	166	165	169
Γ_3	165	159	164	169
Γ_2		157	166	
Γ_5	96	93	80	81
Γ_4	73	79	75	
Γ_3	75	78	73	
Γ_5	46	45	65	59
$\alpha_{Cd\text{-}As}$		26.17	27.80	
$\alpha_{Ge\text{-}As}$		40.26	38.65	
$\beta_{Cd\text{-}As}$		−1.61	2.88	
$\beta_{Ge\text{-}As}$		7.90	2.88	

However, comparing the percentage atomic contributions (PAC's) listed in Table III for $CdGeAs_2$ (this work), $AgGaSe_2$ (Ref. 9), and $CdGeP_2$ (Ref. 10), we note that there is a stronger similarity of $CdGeAs_2$ with $AgGaSe_2$ than with $CdGeP_2$. This is nothing but a direct consequence of the relative values of the atomic masses in the three compounds: 112, 73, and 75 for $CdGeAs_2$ as compared with 108, 70, and 79 for $AgGaSe_2$ and 112, 73, and

TABLE III. Optical frequencies and percentage atomic contributions obtained in this work for $CdGeAs_2$. Also given are similar series of data for $CdGeP_2$ (Ref. 10) and $AgGaSe_2$ (Ref. 9). All results have been obtained using a three-parameter valence-force-field model (see text).

	$CdGeAs_2$				$CdGeP_2$				$AgGaSe_2$			
Mode	ω (cm^{-1})	Cd	Ge (%)	As	ω (cm^{-1})	Cd	Ge (%)	P	ω (cm^{-1})	Ag	Ga (%)	Se
Γ_4	282	1	49	50	399	0	14	86	261	0	54	46
Γ_5	280	1	50	49	394	0	14	86	269	0	58	42
Γ_5	254	5	48	47	356	2	10	88	243	2	62	36
Γ_3	249	3	50	47	353	1	9	90	231	1	59	40
Γ_2					341	0	0	100				
Γ_5	208	34	1	65	300	7	0	93	170	39	1	60
Γ_4	206	27	0	73	307	5	0	95	166	30	0	70
Γ_2	204	0	0	100	278	0	0	100	186	0	0	100
Γ_1	184	0	0	100	306	0	0	100	162	0	0	100
Γ_2	166	0	0	100					186	0	0	100
Γ_5	165	43	45	12	184	26	62	12	140	52	30	36
Γ_3	164	36	43	21	188	17	65	18	133	42	34	24
Γ_5	80	8	41	51	107	9	45	46	62	7	39	54
Γ_4	75	43	23	34	95	22	39	39	59	24	34	42
Γ_3	73	40	18	42	90	48	16	36	58	39	21	40
Γ_5	65	41	8	51	83	45	8	47	53	39	9	52

31 for $CdGeP_2$. This explains why, considering the high-energy bands displayed in Table III, there are nine modes revealed in one work (with 90% anionic PAC's) and four in the two other ones (with only 50% anionic PAC's). Of course, in this case, a second band of five optically active modes comes at slightly lower energy and results clearly from (a) vibrations of the anions against the *heavy* cations (second Γ_4-Γ_5 manifold); (b) the fully symmetric (anionic) Γ_1 mode, and (c) folded longitudinal-acoustic (LA) vibrations including *both* heavy and light cations. This is only because, in $CdGeP_2$, there are mainly anionic vibrations in which there is a first series of nine modes with very similar PAC's and, next, the folded series of LA vibrations well separated in energy. However, even in this case, the hard-bond–smooth-bond features remain. This has been developed at length in Ref. 10 and will not be repeated here. Finally, in all three cases, a last group of four modes is found at low energy. It comes from folded transverse-acoustic (TA) vibrations and, of course, *both* heavy and light cations participate. This results in very similar eigenvectors for all three compounds.

Concerning the weak Raman cross sections noticed for the Γ_3 modes, we find significant anionic PAC's in all three cases (see Table III). For instance, we find 47%, 21%, and 42% for the Γ_3 modes in $CdGeAs_2$ as compared with 50%, 73%, and 34% for the Γ_4 modes. Because most contributions have the same order of magnitude, we cannot explain in this way the very small experimental intensities noticed in Fig. 4. Most probably, this is because of a different origin, $1\Gamma_3[X_3]$ against $2\Gamma_3[W_2]$ modes. In this case, originating from different points of the Brillouin zone, they should experience different electronic excitation processes with different matrix elements and energy denominators. Of course, this was not included in the lattice-dynamics calculation.

Finally, the last point which should be discussed concerns the small Raman cross section noticed in Fig. 3 for four of the six Γ_5 modes. We first note (from Table III) that, except for the mode at 160 cm^{-1}, all theoretical Γ_5 frequencies have noticeable anionic PAC's. This discards the simple explanation suggested in Ref. 19. Moreover, on the experimental side, two modes (the LO-TO doublets at 275–290 cm^{-1} and 259–264 cm^{-1}) have almost identical PAC's and totally different responses (see Fig. 3). This highlights the first-order, folded-zone-like contribution expected from the folded picture of chalcopyrite compounds[1,9] but is inconclusive at the present time. For instance, at low energy, two Γ_5 modes have also a folded-zone-like character and totally different responses. This is because of their different atomic origin (see, again, Table III). One comes from the acoustic branches of InAs and the second from the acoustic branches of GaAs. Altogether, this consideration of Γ_5-mode intensities shows clearly that the difference in experimental responses comes from a complex admixture of differences in electronic excitation processes versus folded-zone-like or first-order-like character. It cannot be understood in light of any simple theoretical approach. The same is true for the intermediate Γ_4-Γ_5 manifold. See, for instance, in Table III, the closely similar anionic *and* cationic contributions displayed for the Γ_4 and Γ_5 modes at 206 and 208 cm^{-1} and the strongly different responses noted in Figs. 2 and 3, respectively.

IV. BOND STRENGTHS IN $CdGeAs_2$ AND RELATED MATERIALS

Up to now we have investigated the long-wavelength phonons of $CdGeAs_2$, both from experimental and theoretical viewpoints. We have compared our work with that reported in Ref. 10 concerning $CdGeP_2$, and showed that, despite significant discrepancies due to the different series of atomic masses, a standard VFF model applied to both cases and fitted with only two bond-stretching and one bond-bending interactions gave a very satisfactory agreement. Since we are dealing every time with 13 experimental frequencies but only three adjustable parameters, this demonstrates that the bonding (and so the lattice dynamics) in ternary pnictides is, to a very large extent, dominated by the interplay of alternating bonds and near-neighbor interactions. In this section we look for more physical insight and attempt to go beyond the empirical (or adjustable parameter) approach. Starting from the change in bond strength through the isoelectronic series: $InGaAs_2$ to $CdGeAs_2$ and $InGaP_2$ to $CdGeP_2$, we show that all parameters obtained in this way correlate directly with the known chemistry of the materials. They are in very good agreement with the prescriptions of a simple Born approximation (Born-Landé) where the local description of valence electrons has been taken into account.[14] This allows simple but accurate molecular predictions to be made for some of the most significant phonons which have a clear chemical origin.

Let us start from a description of the force constants in the pure binary materials. This is by now a well-documented subject[14,20–22] and, using the standard VFF model with the full ZnS-type symmetry and two force constants, one obtains, respectively, for the Ga—P and In—P bonds,[10] (i) for Ga—P, $\alpha=39.2\times10^3$ dyn/cm and $\beta=4.7\times10^3$ dyn/cm; (ii) for In—P, $\alpha=34.8\times10^3$ dyn/cm and $\beta=2.5\times10^3$ dyn/cm. In the same way, using for GaAs and InAs, the experimental inputs of Refs. 23 and 24, respectively, we find (iii) for Ga—As, $\alpha=36.21\times10^3$ dyn/cm and $\beta=4.67\times10^3$ dyn/cm; (iv) for In—As, $\alpha=30.74\times10^3$ dyn/cm and $\beta=1.97\times10^3$ dyn/cm. Comparing these results with the force constants obtained for $CdGeAs_2$ and $CdGeP_2$, with use of the three-parameter model, confirms the following.

(i) A large *increase* in bond strength for the shorter bonds. This is why Ge—As and Ge—P bonds must be termed "hard" when comparing to Ga—As and Ga—P, respectively.

(ii) A smaller *decrease* in both strength for the longer bonds which manifests in both materials (Cd—As and Cd—P with respect to In—As and In—P, respectively).

In other words, in both ternary pnictide analogs of the III-V semiconductors, which we have investigated, the bond strengths vary in the usual way with respect to the related binary materials: the shorter, the stronger. This

is nothing but the natural trend which comes everywhere from the chemistry of the tetrahedral bond.[14,25] Conversely, we have found that all apparent discrepancies, which do exist from compound to compound, come from the relative values of atomic masses. This is, for instance, the relative repartition of modes within a given band which has been discussed at length in Sec. III.

Now, because we know that all force constants must derive from the standard chemistry of the material[14] and because we know that most structural parameters in the binary and ternary semiconductors must be ruled by the conservation of tetrahedral bonds already discussed[5] (CTB), we present a very simple model. We start from the standard Born approximation and write, in light of the CTB,

$$K_r(r_{i,j}) = A/(r_{i,j})^n , \quad (1)$$

where K_r is a purely axial parameter[22,26–28] and $r_{i,j}$ is the sum of Pauling tetrahedral radii[5,25] for the two atoms involved in bond i,j. After simple predictions of the TBM, n is expected to be of order 4. This is because, using universal series of parameters, the covalent (or overlap) energy V_2 for sp^3 hybrids involved in the tetrahedral bond $r_{i,j}$ is independent of the chemical species and is given by[14]

$$V_2 = -3.22\hbar^2/m_e r^2 . \quad (2)$$

The force constant K_r is proportional to the second derivative of the overlap energy versus bond length and, neglecting all effects of polarity and metallization, is given by

$$K = -8V_2/r^2 . \quad (3)$$

Extracting all tetrahedral radii from Ref. 25, we first check Eq. (1) versus the best-fit parameters for GaAs, GaP, InAs, InP, $CdGeAs_2$, and $CdGeP_2$. This is done in Fig. 5 and results in the following.

(i) As far as the bond-length dependence is concerned (slope), we find very satisfactory agreement between our series of fitting parameters and the prediction of the TBM. Within experimental uncertainty, this confirms (demonstrates) that, in numerous tetrahedral semiconductors (*including the ternary pnictides*), all first-nearest-neighbor interactions scale as r^{-4}.

(ii) However, concerning the absolute values, there is about a 30% discrepancy between the predictions of the TBM (dashed line) and the series of axial force constants K_r deduced from the VFF parameters α. From a least-mean-squares-fit using a constant power law (solid line), we find

$$K_r = 4.27\times10^6/[r_{i,j}(\text{Å})]^4 \text{ dyn/cm} , \quad (4)$$

which predicts 120, 142, and 759 N/m for germanium, silicon, and diamond, respectively. This is to be compared with the corresponding experimental values[14] of 128, 160, and 476 N/m. Because this corresponds with bond lengths scaling from 2.44 to 1.54 Å, this gives fair support to our simple empirical approach.

We check now for the internal character of the vibrational modes in the ternary pnictides compounds

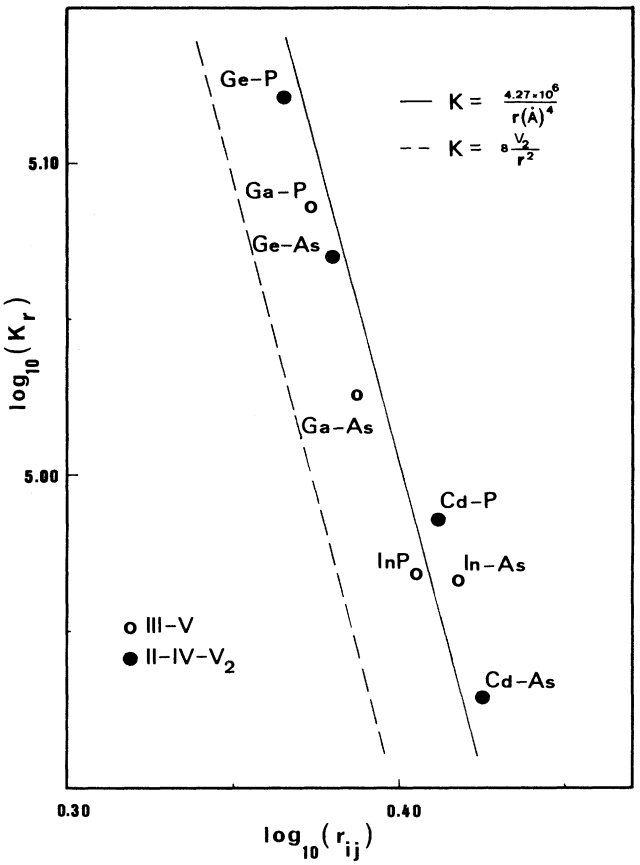

FIG. 5. $\log_{10}$-$\log_{10}$ plot of the bond-stretching force constants K_r (dyn/cm) vs the sum of Pauling tetrahedral radii r_{ij} (Å), for the different series of bonds which define $CdGeAs_2$, $CdGeP_2$, and the related binary materials. All force constants K_r have been deduced from the VFF parameters as described by Musgrave and Pople (Ref. 26).

$A^{II}B^{IV}C_2^V$. Such internal (molecular) modes are well known in α-quartz, for instance, where they come from the stretching and bending vibrations of the constituting SiO_4 tetrahedra.[15,29,30] The same should be true in the ternary pnictides semiconductors but, because there are two different series of constituent tetrahedra, one would expect two different series of stretching frequencies. Because of the small effect of the tetragonal crystal field, this would result in two different Γ_4-Γ_5 manifolds which would characterize the different molecular units. Finally, because we expect all tetrahedral bonds to conserve, independently of the host crystal (CTB), the different frequencies associated with a given pair of atoms should repeat independently of a particular crystal in the family and depend only on the bond length and the reduced mass of vibrating atoms. Roughly speaking, this is nothing but the "hard-bond–smooth-bond" picture and the relative effect of atomic masses already discussed at length in Sec. III. Using Eq. (4) and the standard values of Pauling tetrahedral radii,[25] we first compute, for the tetrahedral modes in $CdGeAs_2$, 281 and 207 cm^{-1} (for the $GeAs_4$ and $CdAs_4$ molecular units, respectively),

which agree satisfactorily with the experimental values, 273–275 and 203–205 cm^{-1} (see Table II). Bearing in mind the crudeness of the model, we find that this result supports very well the molecular approach.

The comparison can be extended to the full series of crystals where experimental data are available and corresponds to the first series of theoretical frequencies listed in Tables IV and V for the IV-V and II-V constituent units, respectively. Comparing with the series of ir and/or Raman frequencies obtained from Refs. 9, 10, 12, 19, and 31–38 for the high- and intermediate-energy Γ_4-Γ_5 manifolds, we find, in both cases, very satisfactory agreement. Moreover, because there is no free parameter, one predicts internal (molecular) frequencies which do not depend on the host compound. This is an independent check of the model which, again, is well satisfied by consideration of the experimental data. This is illustrated in Fig. 6. Clearly, the molecular approach accounts satisfactorily for the chemical trend.

A second set of modes, which can be easily associated with internal molecular vibrations, falls in the low-energy band. Of course, in this case, all modes are dominated by bond-bending interactions but the consideration of PAC's listed in Table III for the two lowest Γ_5 modes suggests that they are mainly associated with pure shear (bending) vibrations of the IV-V and II-V sublattices, respectively. This is consistent with the consideration of atomic vibrations reported for TA(X) modes in ZnS-type semiconductors.[39] In this case, for axially symmetric tensor forces, one expects the bond-bending constants to be[22,28]

$$K_\theta(r_{i,j}) = -K_r(r_{i,j})/(n-1) \ . \tag{5}$$

Using $n=4$, after the Born (TBM) prescriptions, we get for $CdGeAs_2$: 81 and 59 cm^{-1} for the Ge-As and Cd-As sublattices (to be compared with experimental values, 96 and 46 cm^{-1}, respectively). Similar results have been listed in Tables IV and V for the complete series of IV-V and II-V sublattices. We notice, once again, the good agreement observed with the available experimental data.

One can also predict, using the molecular approach, the frequency of the pure Γ_1 anionic modes. In this case all cations are frozen and only the anions vibrate in a totally symmetric fashion. However, because there is already a marked asymmetry in the anion-cation bond strength, one expects the Γ_1 frequency to be controlled

TABLE IV. Comparison of molecular predictions with experimental results for the series of internal modes associated with B—C bonds, in ABC_2 ternary pnictides. In this table, the bond strength decreases from Si—P to Ge—As and the labeling A, B, and C stand for Zn or Cd; Si, Ge, or Sn and P or As, respectively.

B—C elemental bond	Crystal mode	Molecular frequency (cm^{-1})	Experimental frequencies (cm^{-1}) (Zn)BC_2 R	(Zn)BC_2 ir	(Cd)BC_2 R	(Cd)BC_2 ir
Si—P	Γ_4,Γ_5	497	511,511	491,500	488,488	486,486
	Γ_1	343	344		326	
	Γ_5	144	185	185	156	155
			a	b	c	c
Si—As	Γ_4,Γ_5	394	387,402	389,400		
	Γ_1	206	202			
	Γ_5	114	132	131		
			d	d		
Ge—P	Γ_4,Γ_5	392	396,386	392,385	398,387	399,380
	Γ_1	328	328		322	
	Γ_5	113	141	(?)	123	118
			e	f	g	g
Sn—P	Γ_4,Γ_5	318		327	353,340	353,339
	Γ_1	283			301	
	Γ_5	91			93	
				h	i	j
Ge—As	Γ_4,Γ_5	281			273,275	270,272
	Γ_1	197			196	
	Γ_5	81			96	97
					k	l

[a]Reference 31.
[b]Reference 32.
[c]Reference 19.
[d]Reference 33.
[e]Reference 34.
[f]Reference 35.
[g]Reference 10.
[h]Reference 36 (unpolarized).
[i]Reference 37.
[j]Reference 38.
[k]This work.
[l]Reference 12.

TABLE V. Same as Table IV, but now for A—C bonds.

A—C elemental bond	Crystal mode	Molecular frequency (cm^{-1})	Experimental frequencies (cm^{-1}) A(Si)C_2 R	A(Si)C_2 ir	A(Ge)C_2 R	A(Ge)C_2 ir	A(Sn)C_2 R	A(Sn)C_2 ir
Zn—P	Γ_4,Γ_5	368	352,335	347,320	343,(?)	348,330		327
	Γ_1	304						
	Γ_5	106	105		94	80		
			a	b	c	d		e
Cd—P	Γ_4,Γ_5	298	306,(?)	306,285	295,295	300,289	288,280	395,279
	Γ_1	249						
	Γ_5	86	68		64	63	54	
			f	f	g	g	h	i
Zn—As	Γ_4,Γ_5	267	240,230	242,233				
	Γ_1	183						
	Γ_5	77	75					
			j	j				
Cd—As	Γ_4,Γ_5	207			205,203	202,199		
	Γ_1	160						
	Γ_5	59			46	42		
					k	l		

[a]Reference 31.
[b]Reference 32.
[c]Reference 34.
[d]Reference 35.
[e]Reference 36 (unpolarized).
[f]Reference 19.
[g]Reference 10.
[h]Reference 37.
[i]Reference 38.
[j]Reference 33.
[k]This work.
[l]Reference 12.

more by the *hard* bond vibrations. This is indeed what is found. Our calculation predicts 197 cm^{-1} for $GeAs_4$ molecular units in $CdGeAs_2$, which is to be compared with an experimental value of 196 cm^{-1} (see Table II). The corresponding series of predicted values, for all IV-V and II-V molecular units of experimental interest, are given in Tables IV and V, respectively. This demonstrates that, systematically, the experimental value for a given compound correlates with the IV-V constituent units.

The association of molecular vibrations with the remaining modes in the central energy band is not so easy. This is because different bending and stretching interactions compete in a real crystal and result in *external* vibrations[29] which have no molecular character and are specific for a given compound. Of course, these modes are not controlled by one single bond but, from small variations of the force constants, we have found that they are mainly dominated by bond-stretching interactions. Returning to $CdGeAs_2$, a close examination of PAC's listed in Table III suggests that the lowest Γ_3-Γ_5 modes in the midband come from the stretching vibrations of the Cd-As against Ge-As sublattices. This is nothing but the stretching counterpart of the low-frequency Γ_5 components. From the calculation, we get 169 cm^{-1}, to be compared with 160 and 165 cm^{-1} for the Γ_3 and Γ_5 modes, respectively. Again, this result supports the

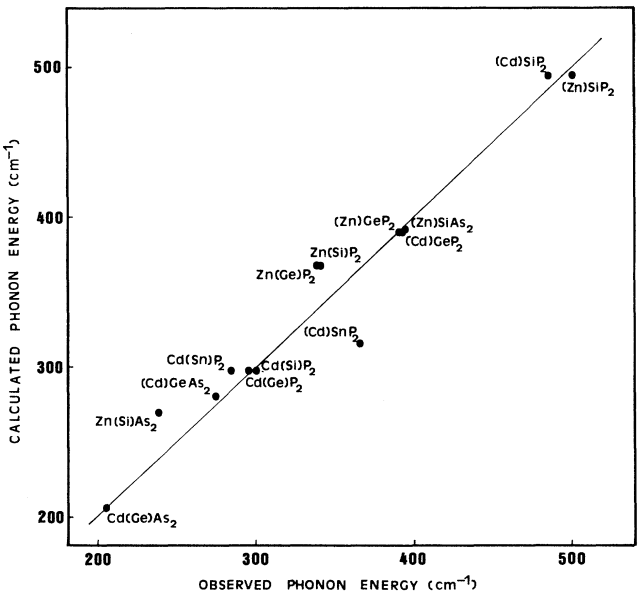

FIG. 6. Correlation between the series of Raman and/or infrared Γ_{15}-like frequencies predicted for A-C_4 and B-C_4 molecular units with the experimental values (see text). For clarity, the active bond has been identified by using notations $A(B)C_2$ or $(A)BC_2$, respectively.

TABLE VI. External modes for ABC_2 sublattices (see text).

External mode	Crystal symmetry	Molecular frequency (cm^{-1})	Experimental frequencies (cm^{-1}) R	ir
Si—P/Zn—P	Γ_3,Γ_5	296	(?),270 [a]	260 [b]
Si—P/Cd—P	Γ_3,Γ_5	257	301,252 [c]	252 [c]
Ge—P/Zn—P	Γ_3,Γ_5	247	247,203 [d]	202 [e]
Si—As/Zn—As	Γ_3,Γ_5	217	240,204 [f]	207 [f]
Sn—P/Zn—P	Γ_3,Γ_5	212		
Ge—P/Cd—P	Γ_3,Γ_5	211	228,184 [g]	187 [g]
Sm—P/Cd—P	Γ_3,Γ_5	177	265,146 [h]	
Ge—As/Cd—As	Γ_3,Γ_5	169	160,165 [i]	157 [j]

[a]Reference 31.
[b]Reference 32.
[c]Reference 19.
[d]Reference 34.
[e]Reference 35.
[f]Reference 33.
[g]Reference 10.
[h]Reference 37.
[i]This work.
[j]Reference 12.

molecular model.

Similar results are listed in Table VI for most members of the ternary pnictide family. Again notice the good overall agreement. For convenience, a systematic comparison of the series of molecular frequencies obtained in this work with the results of the three-parameter VFF model is shown in Table II. It supports the surprising agreement achieved using this simple approach and can be easily generalized, using the data of Tables IV–VI, to all crystals of the same family.

V. CONCLUSION

By investigating the long-wavelength phonons in $CdGeAs_2$, we could resolve all optically active frequencies predicted from group-theory arguments. Next, discussing the results in light of the VFF model (with only three adjustable parameters) we could get a very satisfactory agreement. Performing a comparison with the parent compound $CdGeP_2$, it was found that, in both cases, very similar trends rule the renormalization of the force constants with respect to the fictitious $A^{III}B^{III}C_2^{V}$ materials and that all apparent discrepancies come from the relative values of atomic masses. Finally, we could set a simple molecular model. Performing a systematic comparison with the simple predictions of the semiempirical TBM, we could show that there is an inverse scaling law of the bond strengths versus the fourth power of the bond lengths. Working in light of the CTB and starting from the eigenmodes obtained from the lattice-dynamics calculation, we confirmed most features of the hard-bond–smooth-bond picture. The upper Γ_4-Γ_5 manifold is always governed by molecular stretching vibrations of the light cation and anion together (hard bond). The second Γ_4-Γ_5 doublet comes from molecular vibrations of the heavy cation and anion together (smooth bond). In between, there is a Γ_1 mode due essentially to stretching anions against the frozen light cations (hard bond) and two modes of stretching II-V against IV-V units (mixed character). Finally, the low-energy bands also possess a clear molecular character but originate from the shear vibrations of II-V and IV-V sublattices, respectively.

ACKNOWLEDGMENTS

We gratefully acknowledge R. S. Feigelson for providing us with the $CdGeAs_2$ crystal used in this work. We also thank M. Galtier, from the Groupe de Dynamique des Phases Condensées (USTL), for expert assistance with the IRFT spectrometer. Finally, one of us (L.A.) thanks M. Cardona and the Max Planck Institute for the use of the Raman facility. This work was supported in part by the Comisión Interministérial de Ciencia y Tecnologia (Spain).

[1]See, for instance, J. L. Shay and J. E. Wernick, *Ternary Chalcopyrite Semiconductors: Growth, Electronic Properties and Applications* (Pergamon, New York, 1975).

[2]See, for instance, M. A. Shahid and S. Mahajan, Phys. Rev. B **38**, 1344 (1988); also see A. Mascarenhas and J. M. Olson, *ibid.* **41**, 9947 (1990).

[3]See, for instance, T. Kurimoto and N. Hamada, Phys. Rev. B **40**, 3889 (1989); also see R. Magri and C. Calandra, *ibid.* **40**,

3896 (1989).
[4]M. Razeghi, *A Survey of GaInAsP/InP for Photonic and Electronic Applications, The MOCVD Challenge* (Hilger, Bristol, 1989), Vol. 1.
[5]J. E. Jaffe and A. Zunger, Phys. Rev. B **29**, 1882 (1984).
[6]J. E. Jaffe and A. Zunger, Phys. Rev. B **28**, 5822 (1983).
[7]J. E. Jaffe and A. Zunger, Phys. Rev. B **30**, 741 (1984).
[8]A. Zunger and J. E. Jaffe, Phys. Rev. Lett. **51**, 662 (1983); also see J. E. Jaffe and A. Zunger, Phys. Rev. B **27**, 5176 (1983).
[9]J. Camassel, L. Artus, and J. Pascual, Phys. Rev. B **41**, 5717 (1990); also see L. Artus, J. Pujol, J. Pascual, and J. Camassel, Phys. Rev. **41**, 5727 (1990).
[10]L. Artus, J. Pascual, J. Pujol, and J. Camassel, Phys. Rev. B **43**, 2088 (1991).
[11]G. D. Holah, A. Miller, W. D. Dunnet, and G. W. Iseler, Solid State Commun. **23**, 75 (1975).
[12]L. Artus, J. Pascual, and J. Camassel, Mater. Sci. Eng. B **5**, 239 (1990).
[13]J. Pujol, L. Artus, J. Pascual, and J. Camassel, Phys. Scr. **41**, 696 (1990).
[14]W. A. Harrison, *Electronic Structure and the Properties of Solids: The Physics of the Chemical Bond* (Freeman, San Francisco, 1980); see also Phys. Rev. B **27**, 3592 (1983).
[15]J. Camassel, A. Goullet, and. J. Pascual, Phys. Rev. B **38**, 8419 (1988).
[16]*Numerical Data and Functional Relationships in Science and Technology*, edited by K. H. Hellwege, Landolt-Börnstein, New Series, Vol. 17 (Springer, Berlin, 1982); also see A. Shileika, Surf. Sci. **37**, 730 (1973).
[17]C. Varea de Alvarez and M. Cohen, Phys. Rev. Lett. **30**, 979 (1973).
[18]L. Artus, Y. Bertrand, C. Ance, and A. Lopez, Solid State Commun. **57**, 649 (1986); also see Prog. Cryst. Growth Charact. **10**, 257 (1984).
[19]M. Bettini, W. Bauhofer, M. Cardona, and R. Nitsche, Phys. Status Solidi B **63**, 641 (1974).
[20]P. N. Keating, Phys. Rev. **145**, 637 (1966).
[21]E. O. Kane, Phys. Rev. B **31**, 7865 (1985).
[22]M. Born and K. Huang, *Dynamical Theory of Crystal Lattices* (Oxford University Press, London, 1954).
[23]D. Strauch and R. Dorner, J. Phys. Condens. Matter **2**, 1457 (1990).
[24]R. Carles, N. Saint-Cricq, J. B. Renucci, M. A. Renucci, and A. Zwick, Phys. Rev. B **22**, 4804 (1980).
[25]L. Pauling, *The Nature of the Chemical Bond* (Cornell University Press, Ithaca, New York, 1957).
[26]M. J. P. Musgrave and J. A. Pople, Proc. R. Soc. London Ser. A **268**, 474 (1962).
[27]R. M. Martin, Phys. Rev. B **1**, 4005 (1970).
[28]J. Pascual, J. Camassel, P. Merle, and H. Mathieu, Phys. Rev. B **21**, 2439 (1980).
[29]F. Matossi, J. Chem. Phys. **17**, 679 (1949).
[30]A. Goullet, J. Pascual, R. Cusco, and J. Camassel (unpublished).
[31]I. P. Kaminow, E. Buehler, and J. H. Wernick, Phys. Rev. B **2**, 960 (1970).
[32]G. D. Holah, J. Phys. C **5**, 1893 (1972).
[33]W. H. Koschel, F. Sorger, and J. Baars, Solid State Commun. **15**, 719 (1974).
[34]M. Bettini and A. Miller, Phys. Status Solidi B **66**, 579 (1974).
[35]A. Miller, G. D. Holah, and W. C. Clark, J. Phys. Chem. Solids **35**, 685 (1974).
[36]L. B. Zlatkin, J. F. Markov, A. I. Stekhanov, and M. S. Shur, Phys. Status Solidi B **32**, 473 (1969).
[37]G. Irmer, A. Heinrich, and J. Monecke, Phys. Status Solidi B **132**, 93 (1985).
[38]Y. F. Markov and N. B. Reshetnyak, Opt. Spektrosk. **33**, 280 (1972) [Opt. Spectrosc. (USSR) **33**, 520 (1972)].
[39]R. Roman and J. Pascual, Phys. Scr. **38**, 729 (1988).